# $\pi^- p \to \pi^- \pi^0 p$ Reaction at 2.77 GeV/$c$ for Low Momentum Transfers to the Proton

J. P. Baton and G. Laurens
*Département de Physique des Particules Elémentaires, Centre d'Etudes Nucléaires, Saclay, France*
(Received 1 March 1968)

The reaction $\pi^- p \to \pi^- \pi^0 p$ produced by 2.77-GeV/$c$ pions has been studied for low squared four-momentum transfers to the proton ($\Delta^2 \leqslant 13\mu^2$). A selection based on a fast premeasurement method has allowed the accumulation of high statistics (7666 events) and a detailed study of the $\rho^-$ properties. In particular, the $\rho^-$ mass and width are determined as a function of $\Delta^2$, showing essentially no variation of these parameters in the whole $\Delta^2$ range. On the other hand, the mass and width values deduced from the mass spectra ($\omega_r = 773 \pm 2$ MeV, $\Gamma_r = 150 \pm 5$ MeV) differ from the corresponding values for the resonant $P$ wave ($\omega_r = 755 \pm 5$ MeV, $\Gamma_r = 110 \pm 9$ MeV) obtained by extrapolation to the pion pole, following the Chew-Low method. Essential results on the $\pi^-\pi^0$ elastic cross section are summarized. The sensitivity of the determination of the $\rho^-$ production and decay parameters to various mass and $\Delta^2$ cuts is shown.

## I. INTRODUCTION

MANY experiments have been carried out during recent years in order to study $\pi\pi$ scattering with the one-pion-exchange (OPE) model[1] by means of the two reactions

$$\pi^- p \to \pi^- \pi^0 p, \tag{1}$$

$$\pi^- p \to \pi^+ \pi^- n. \tag{2}$$

However, despite the large number of events measured, the final statistics have never allowed the rigorous use of the OPE, i.e., the extrapolation of the experimental data at the pole of the transition matrix element. Instead, corrective form factors have been introduced into the OPE model[2] or strong modifications have been made to it by including absorption effects (OPEA model).[3]

To perform the extrapolation suggested by Chew and Low,[1] we have undertaken a new experiment $\pi^- p \to \pi^- \pi^0 p$ with the purpose of reaching statistics larger by an order of magnitude than those obtained in previous experiments.

140 000 pictures have been taken with the 2-m CERN hydrogen bubble chamber exposed to a (2.77±0.010)-GeV/$c$ $\pi^-$ beam. The results on the extrapolated values of the $\pi\pi$ scattering parameters have been published previously.[4] In this paper we shall analyze the experimental aspects of this work, in particular the different problems raised by the large number of data, and discuss other results on the $\rho^-$ properties in the physical region.

## II. SELECTION OF EVENTS

In order to reduce the number of measurements, we have limited the study of reaction (1) to $\Delta^2$ values less than $13\mu^2$ ($\Delta^2$ is the squared four-momentum transfer, and $\mu$ the charged pion mass), i.e., to proton momenta less than 520 MeV/$c$ in the laboratory. On the other hand, during the scanning we have separated reaction (1) from reaction (2) and above all from the elastic scattering,

$$\pi^- p \to \pi^- p, \tag{3}$$

whose cross section is six times larger than that of reaction (1) for $\Delta^2 \leqslant 13\mu^2$. The following procedure was used:

(a) Only the two-prong events with a heavily ionizing positive track were retained. This eliminates most of the events of reaction (2).

(b) For the selected events, the curvature of the positive track (or its length if the track stopped in the chamber) and also its angle with the incident track were measured on the scanning table. With this information a geometrical reconstruction program, ELIM, classified the events as belonging to reaction (1) or (3). This premeasurement method had already been used in a previous experiment.[5]

In this way, among the 181 000 two-prong events scanned, 73 790 have been premeasured. ELIM has classified 38 620 events belonging to reaction (3), and 7030 to reaction (1) but with the momentum of the positive track greater than 560 MeV/$c$.

Finally, 28 100 events representing only 16% of the two-prong interactions were carefully measured, with four measuring machines on line to a CAE 510 computer.[6] Figure 1 shows the results of the premeasurement; its efficiency and usefulness appear clearly.

After full measurement, the events have been computed with the THRESH and GRIND programs. After checking the ionization, 9860 events have been identified as belonging to reaction (1). For a final selection, an event was constrained to have

(a) the momentum of its positive track less than 520 MeV/$c$ ($\Delta^2 \leqslant 13\mu^2$),

(b) a squared missing mass between $-3\mu^2$ and $5\mu^2$,

(c) a $\chi^2$ value less than 6.

[1] G. F. Chew and F. E. Low, Phys. Rev. **113**, 1640 (1959).
[2] F. Selleri, Phys. Letters **3**, 76 (1962).
[3] K. Gottfried and J. D. Jackson, Nuovo Cimento **34**, 735 (1964); J. D. Jackson, Rev. Mod. Phys. **37**, 484 (1965).
[4] J. P. Baton, G. Laurens, and J. Reignier, Nucl. Phys. **B3**, 349 (1967); Phys. Letters **25B**, 419 (1967).
[5] J. P. Baton, Commissariat à l'Energie Atomique Report No. R-3291 (unpublished).
[6] B. Deler, Commissariat à l'Energie Atomique Report No. R-2717 (unpublished).

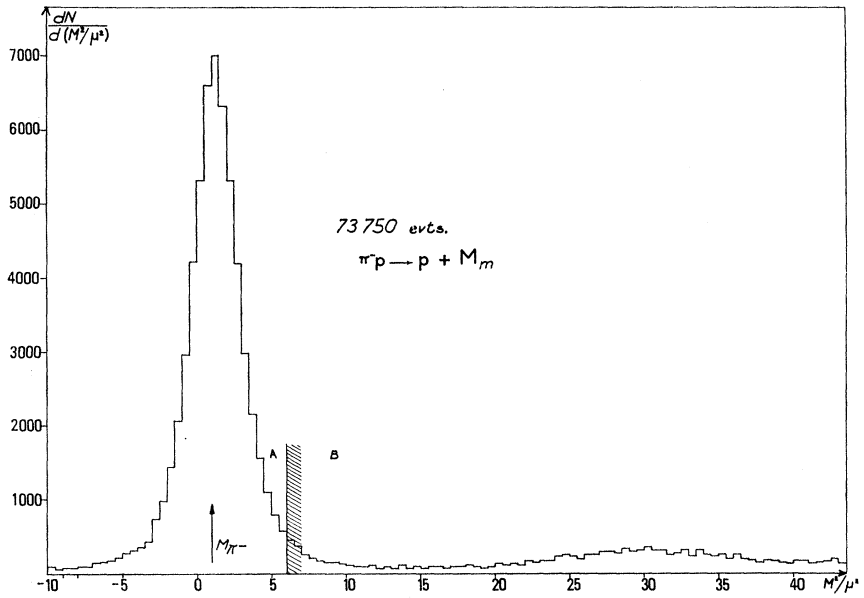


FIG. 1. Distribution of the unfitted squared mass associated with the proton resulting from the premeasurement of reaction $\pi^- p \to p + M$ (in units of $\mu^2$). Events located in region A have been classified as elastic; in region B they have been classified as inelastic.

7666 events fulfilling these three conditions constitute our final sample. Figure 2 shows the squared missing-mass distribution of these events.

It should be noticed that, because of the selection method based on a premeasurement on the scanning table, some events with a dipion mass less than 450 MeV have been lost. In fact, we have classified as elastic the events for which the square of the mass associated with the proton is less than $6\mu^2$ (Fig. 1); as a consequence, a small number of events belonging to reaction (1) with a low dipion mass have been classified arbitrarily as elastic events. Measurements performed on a sample of events located in the ambiguous region have allowed an estimate of this loss [hatched events on Fig. 4(a)].

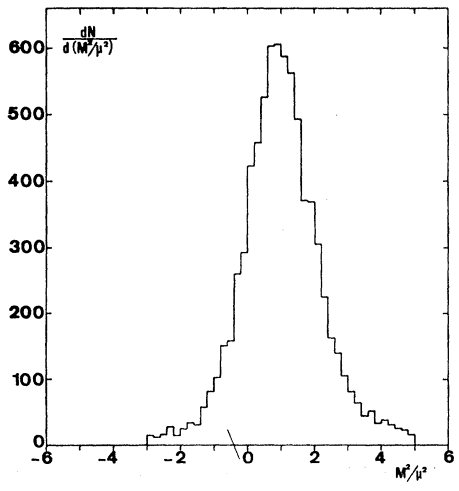


FIG. 2. Distribution of the squared missing mass for reaction (1) (in units of $\mu^2$).

## III. DETERMINATION OF PRODUCTION CROSS SECTION

For a correct evaluation of the $\pi\pi$ elastic scattering cross section, one needs a precise knowledge of the production cross section of reaction (1). In order to obtain this value, we have measured in a sample of films about 4000 already premeasured elastic events. Then, assuming that in the diffraction peak region the elastic differential cross section may be represented by

$$\frac{d\sigma}{d\Delta^2} = \left(\frac{d\sigma}{d\Delta^2}\right)_{\Delta^2=0} e^{-A\Delta^2}, \tag{4}$$

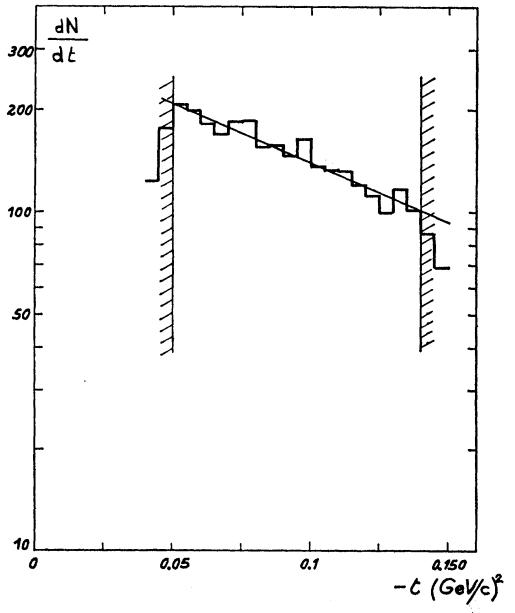


FIG. 3. Distribution of the elastic differential cross section; the straight line represents a least-squares fit to the data.

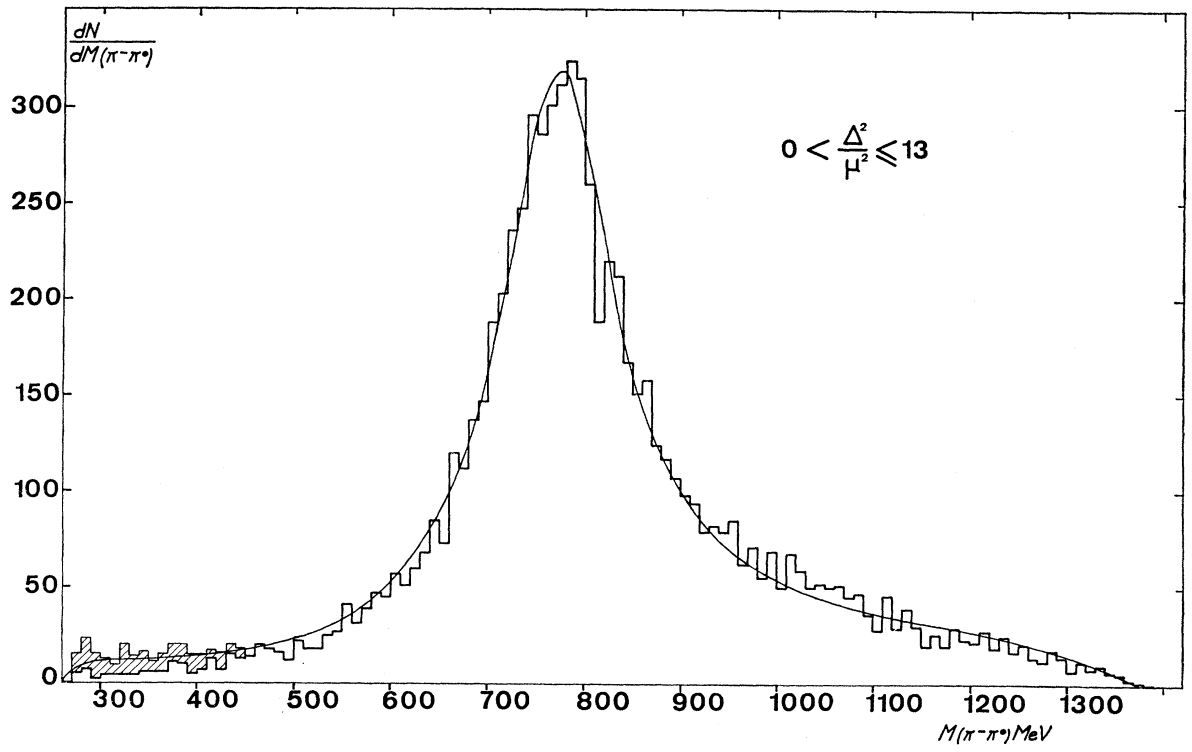


(a)

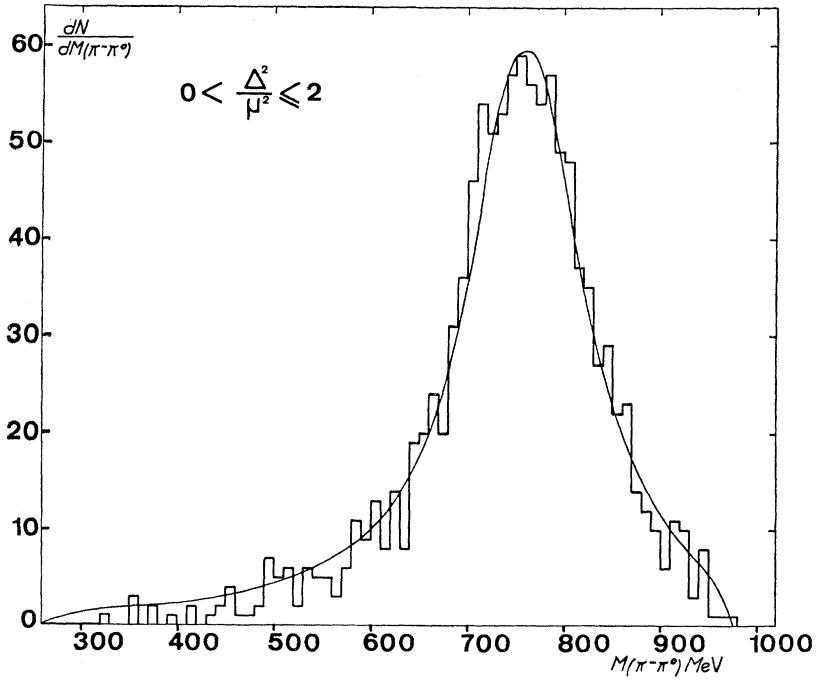


(b)

FIG. 4. $(\pi^-\pi^0)$ mass spectra for different $\Delta^2$ intervals; solid curves represent a least-squares fits of (Breit-Wigner)+(phase-space) curves. (a) $0<\Delta^2/\mu^2\leqslant 13$, 7666 events (it is considered that in the hatched region, events have been lost at the scanning premeasurement step), (b) $0<\Delta^2/\mu^2\leqslant 2$, 1112 events, (c) $2<\Delta^2/\mu^2\leqslant 4$, 1776 events, (d) $4<\Delta^2/\mu^2\leqslant 6$, 1522 events, (e) $6<\Delta^2/\mu^2\leqslant 9$, 1699 events, (f) $9<\Delta^2/\mu^2\leqslant 13$, 1527 events.

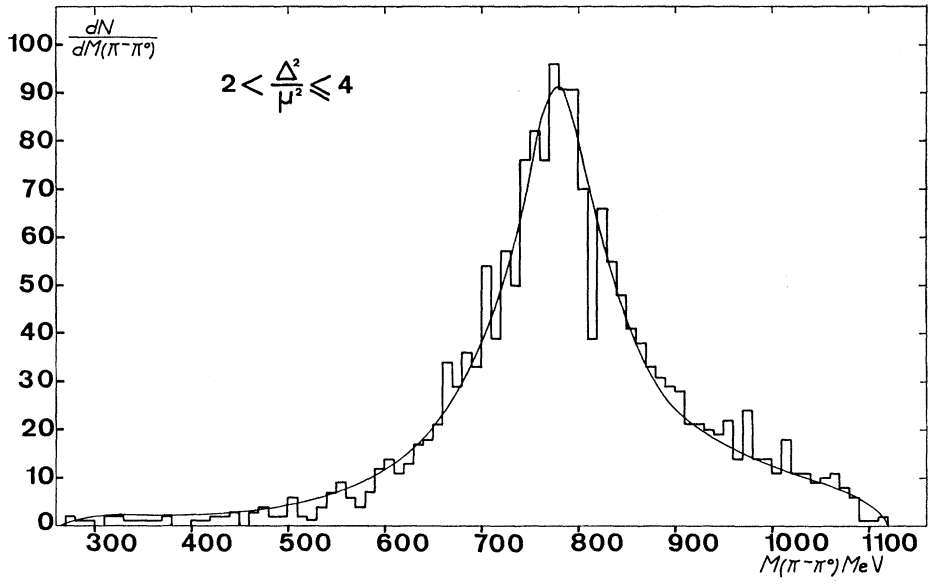


(c)

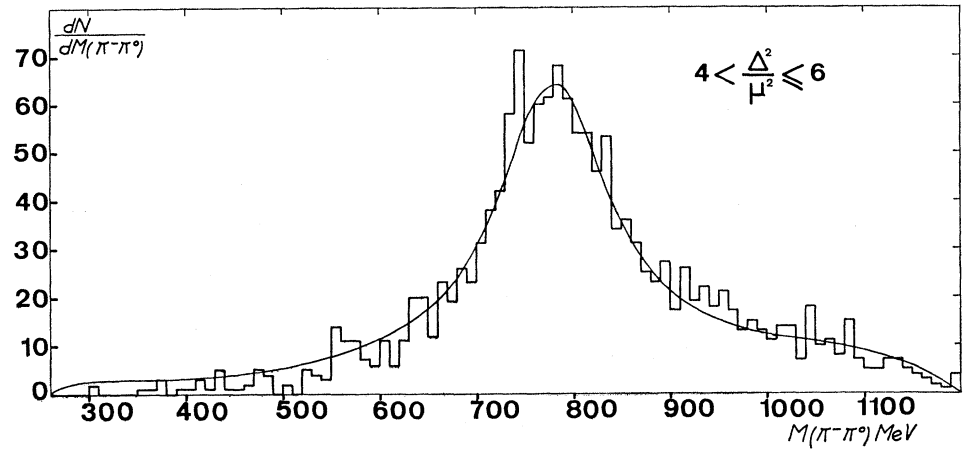


(d)

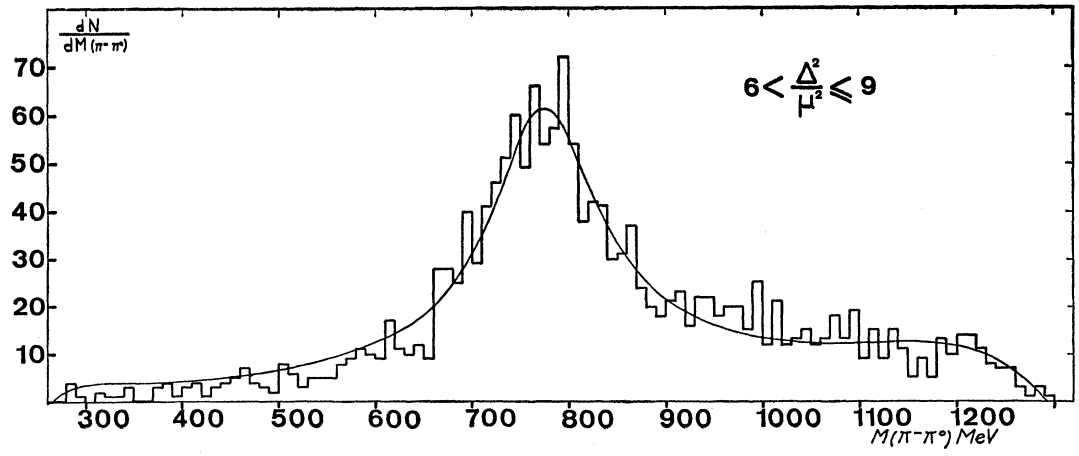


(e)

FIG. 4. (*continued*)

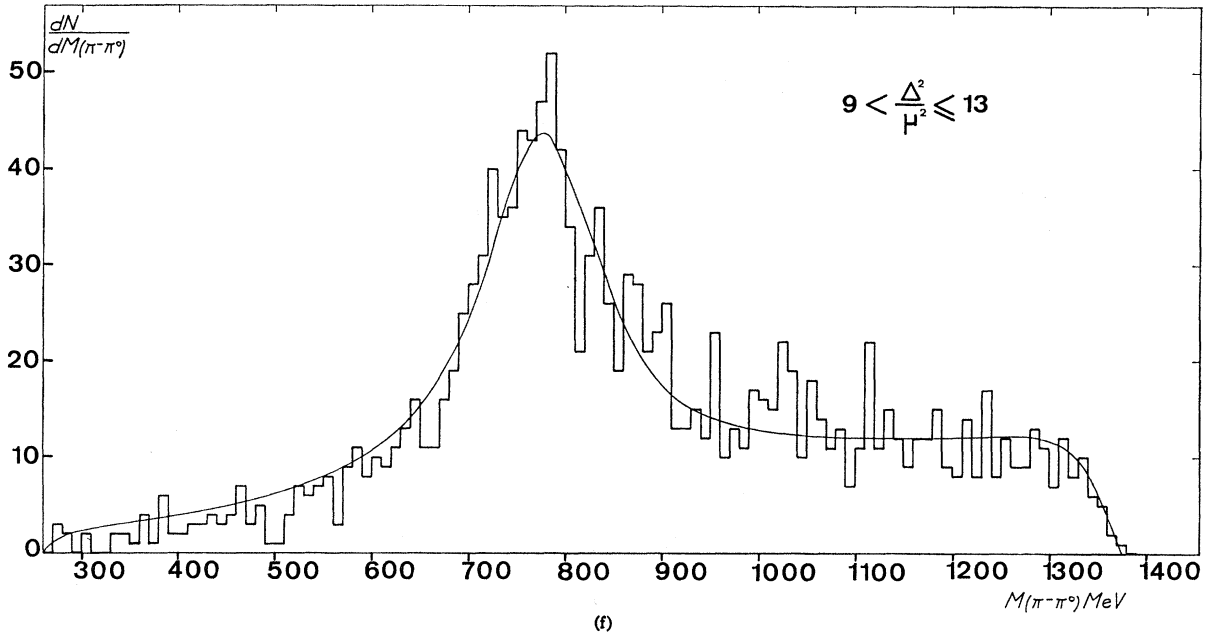


(f)

FIG. 4. (*continued*)

where $(d\sigma/d\Delta^2)_{\Delta^2=0}$, the differential cross section at 0°, is given by the optical theorem, one obtains[7]

$$(d\sigma/d\Delta^2)_{\Delta^2=0}=55.25\pm0.01 \text{ mb}/(\text{GeV}^2/c^2).$$

This value is indeed very close to the one obtained by extrapolating down to $\Delta^2=0$ the value of $d\sigma/d\Delta^2$.[8,9] The coefficient $A$, given by the slope of the distribution $\ln(dN/d\Delta^2)$ (Fig. 3), is determined from a sample $N_1$ of elastic events for which $0.05\ (\text{GeV}/c)^2\leqslant\Delta^2\leqslant0.14\ (\text{GeV}/c)^2$. One finds

$$A=7.8\pm0.25\ (\text{GeV}/c)^{-2},$$

and Eq. (4) becomes

$$d\sigma/d\Delta^2=(55.25\pm0.01)\times e^{-(7.8\pm0.25)\Delta^2}.$$

By integration between the two limits of $\Delta^2$, one obtains

$$\sigma_{el}=\int_{\Delta^2=0.05}^{\Delta^2=0.14}(55.25\pm0.01)e^{-(7.8\pm0.25)\Delta^2}$$

$$=2.42\pm0.06 \text{ mb}.$$

To this number $N_1$ of elastic events corresponded a known number $N_2$ of events of reaction (1). Then, for $\Delta^2\leqslant13\mu^2$,

$$\sigma_{\pi^-\pi^+p}=\sigma_{el}(N_2/N_1)=(2.42\pm0.06)(N_2/N_1)$$

$$=1.15\pm0.07 \text{ mb}.$$

The error takes into account the statistical error as well as the error in the determination of $A$ and $(d\sigma/d\Delta^2)_{\Delta^2=0}$.

## IV. MASS SPECTRA

### A. $\rho^-$ Mass and Width

The large number of events has allowed a precise study of the $\rho^-$ mass and width as a function of $\Delta^2$. Figures 4(a)–4(f) show the dipion mass spectra for different $\Delta^2$ intervals.

To estimate the $\rho^-$ mass and width, we have made a least-squares fit to the effective-mass spectra of the function

$$F=\alpha f_{BW}(\omega)\lambda_1(\omega)+(1-\alpha)f_{bg}(\omega)\lambda_2(\omega), \qquad (5)$$

where $f_{BW}(\omega)$ is a Breit-Wigner curve,[10] represented by

$$f_{BW}(\omega)=\frac{\omega_r^2\Gamma^2(\omega)}{(\omega_r^2-\omega^2)^2+\omega_r^2\Gamma^2(\omega)}$$

with

$$\Gamma(\omega)=\Gamma_r\left(\frac{\omega^2-4\mu^2}{\omega_r^2-4\mu^2}\right)^{3/2}\frac{\omega_r}{\omega}.$$

$\Gamma_r$ and $\omega_r$ are the $\rho^-$ width and mass; $f_{bg}(\omega)$ is the nonresonant background; $\alpha$ is the percentage of $\rho^-$ produced; $\lambda_1(\omega)$ and $\lambda_2(\omega)$ are corrective terms of the form

$$\lambda_i(\omega)=\int_{\Delta_{min}^2(\omega)}^{\Delta_{max}^2(\omega)}e^{-B_i\Delta^2}d\Delta^2,$$

taking into account the kinematical limit of the

[7] A. Citron, W. Galbraith, T. F. Kycia, B. A. Leontic, R. M. Phillips, and A. Rousset, Phys. Rev. Letters 13, 204 (1964).
[8] M. L. Perl, L. W. Jones, and C. C. Ting, Phys. Rev. 132, 1252 (1963).
[9] L. D. Jacobs, thesis, University of California, Berkeley, 1966 (unpublished).
[10] J. D. Jackson, Nuovo Cimento 34, 1644 (1964).

Chew-Low plot, and the exponential dependence of the dipion production angular distribution, inside the $\rho^-$ for $\lambda_1$, outside the $\rho^-$ for $\lambda_2$, which is of the form $d\sigma/d\Delta^2 = K \exp(-B_i\Delta^2)$. At our energy, $B_1 = 8.2$ $(\mathrm{GeV}/c)^{-2}$, $B_2 = 4.5$ $(\mathrm{GeV}/c)^{-1/2}$. (See Sec. VI below for the determination of $B_1$ and $B_2$.) The values obtained for $\omega_r$ and $\Gamma_r$ are summarized in Table I.

One notices that the introduction of the corrective factors $\lambda_1(\omega)$ and $\lambda_2(\omega)$ has the following effects:

(a) to give for the lower interval in $\Delta^2$, a $\rho^-$ mass value comparable to those of the other intervals; this is not the case when these corrective factors are neglected[11] (Table I, second part);

TABLE I. $\rho^-$ mass, width, and relative production cross section for different $\Delta^2$ cuts; for the definition of $\lambda_i$ see text (IV A).

| | | Without $\lambda_i$ correction | | | With $\lambda_i$ correction | | |
|---|---|---|---|---|---|---|---|
| $\Delta^2/\mu^2$ | Number of events | Mass $\rho^-$ (MeV) | Width $\rho^-$ (MeV) | % of $\rho^-$ | Mass $\rho^-$ (MeV) | Width $\rho^-$ (MeV) | % of $\rho^-$ |
| 0– 2 | 1112 | 748±3 | 100± 5 | >99 | 772±3 | 154±7 | >99 |
| 0– 4 | 2888 | 762±3 | 114± 8 | 90±4 | 775±2 | 159±6 | 96±3 |
| 0– 6 | 4440 | 766±3 | 127± 6 | 92±5 | 776±2 | 159±5 | 91±4 |
| 0– 9 | 6139 | 766±2 | 127± 8 | 87±4 | 774±2 | 155±5 | 85±4 |
| 0–13 | 7666 | 767±2 | 146±12 | 85±3 | 773±1 | 150±5 | 77±6 |
| 2– 4 | 1776 | 770±2 | 120± 5 | 94±3 | 776±3 | 156±5 | 94±3 |
| 4– 6 | 1552 | 773±2 | 123± 8 | 88±3 | 778±3 | 157±6 | 85±3 |
| 6– 9 | 1699 | 767±3 | 126± 8 | 71±3 | 772±3 | 154±6 | 70±2 |
| 9–13 | 1527 | 764±4 | 140±12 | 50±2 | 770±4 | 148±7 | 49±3 |

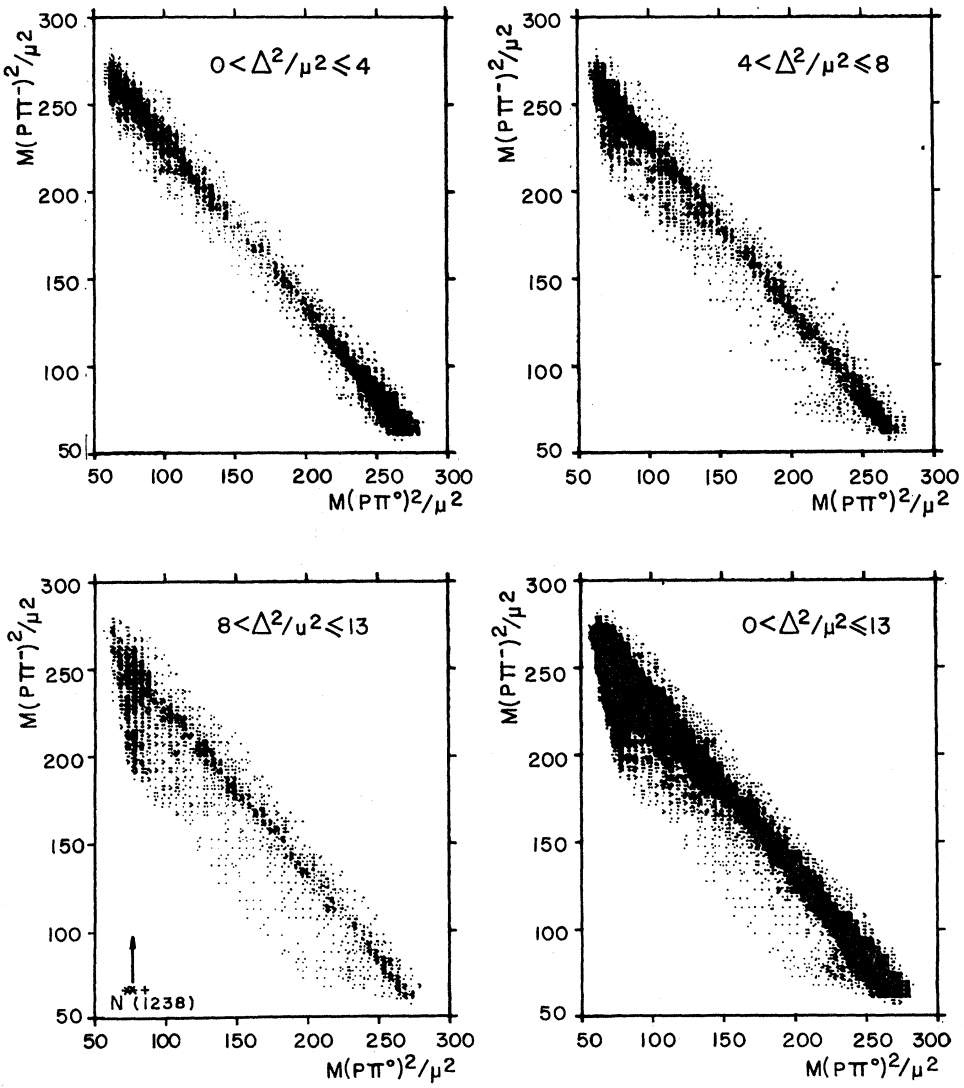


FIG. 5. Dalitz plots of reaction $\pi^- p \to \pi^- \pi^0 p$ for (a) $0<\Delta^2/\mu^2\leqslant 4$, (b) $4<\Delta^2/\mu^2\leqslant 8$, (c) $8<\Delta^2/\mu^2\leqslant 13$, (d) $0<\Delta^2/\mu^2\leqslant 13$.

[11] M. Roos, Nucl. Phys. B2, 615 (1967).

(b) to give a $\rho^-$ mass value systematically higher than the one obtained previously in similar experiments[12,13];
(c) to increase the width of the $\rho^-$ meson.

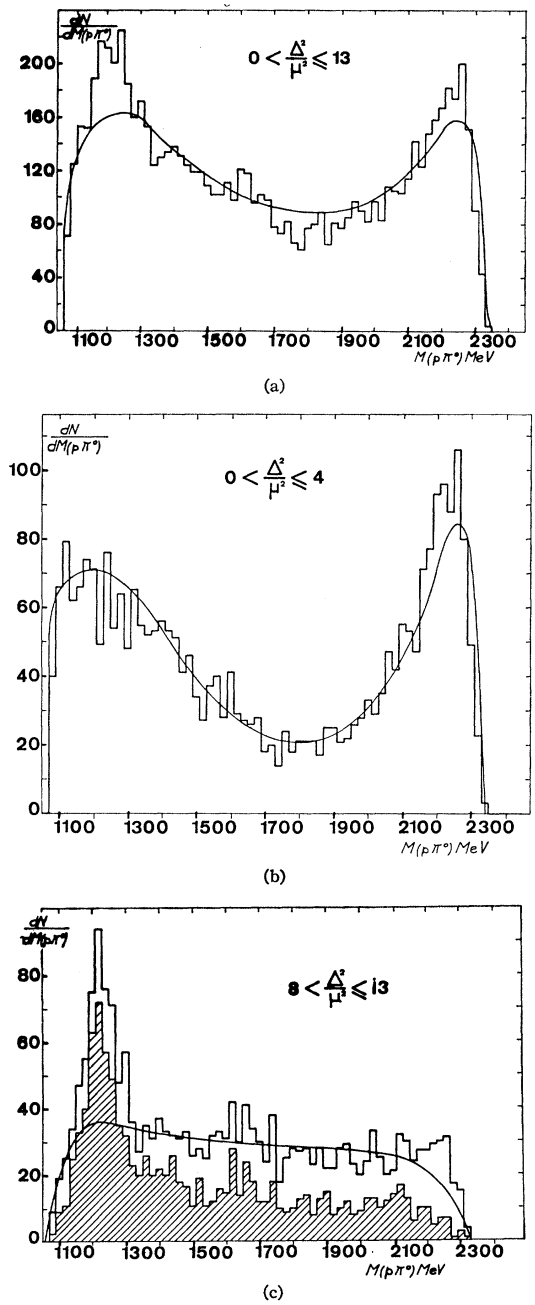


FIG. 6. ($p\pi^0$) mass spectra for different $\Delta^2$ intervals. Fitted curves represent invariant phase-space distributions modified by the $\rho^-$ reflection. (a) $0<\Delta^2/\mu^2\leqslant 13$, (b) $0<\Delta^2/\mu^2\leqslant 4$, (c) $8<\Delta^2/\mu^2\leqslant 13$. The hatched distribution represents the ($p\pi^0$) mass spectrum outside the $\rho^-$ region ($M_{\pi^-\pi^0}\leqslant 660$ MeV, $M_{\pi^-\pi^0}\geqslant 860$ MeV).

[12] V. Hagopian, W. Selove, J. Alitti, J. P. Baton, and M. Neveu-Rene, Phys. Rev. **145**, 1128 (1966).
[13] D. H. Miller, L. Gutay, P. B. Johnson, F. J. Loeffler, R. L. McIlwain, R. J. Sprafka, and R. B. Willmann, Phys. Rev. **153**, 1423 (1967).

On the other hand, the mean values of the mass $\omega_r=773\pm 2$ MeV and of the width $\Gamma_r=150\pm 5$ MeV should be compared with the value obtained from our phase-shift analysis by extrapolation at $\Delta^2=-\mu^2$. By this method, which insures a rigorous determination of the position of the pole of the $S$ matrix in the complex plane of the energy, the $\rho$ resonance is situated at

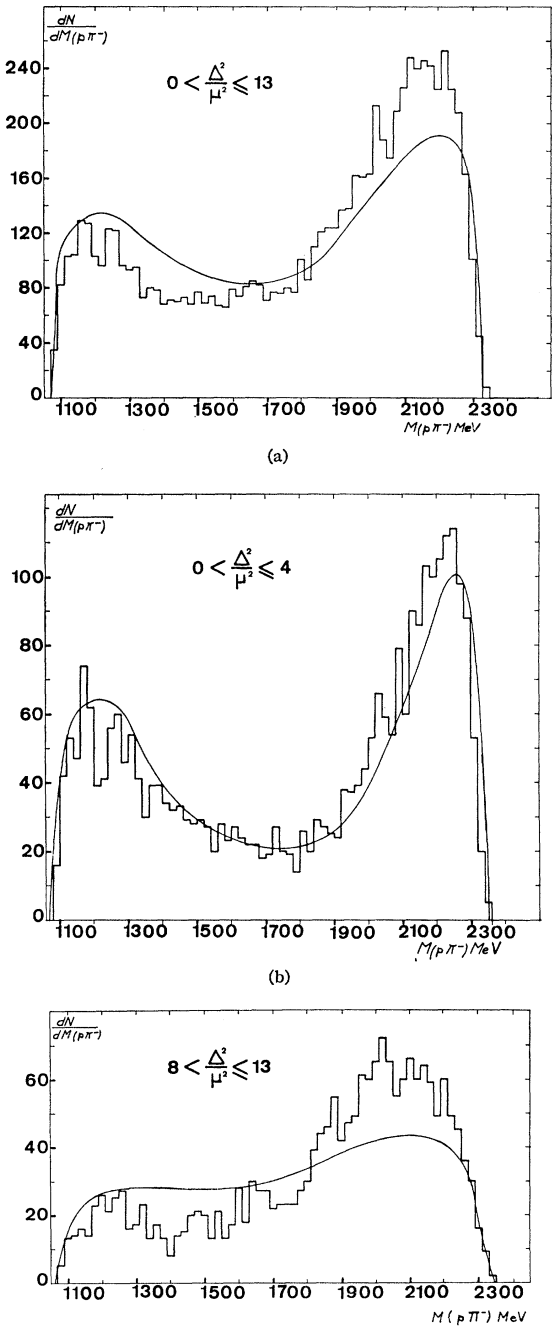


FIG. 7. ($p\pi^-$) mass spectra for different $\Delta^2$ intervals. Fitted curves represent invariant phase distributions modified by the $\rho^-$ reflection. (a) $0<\Delta^2/\mu^2\leqslant 13$, (b) $0<\Delta^2/\mu^2\leqslant 4$, (c) $8<\Delta^2/\mu^2\leqslant 13$.

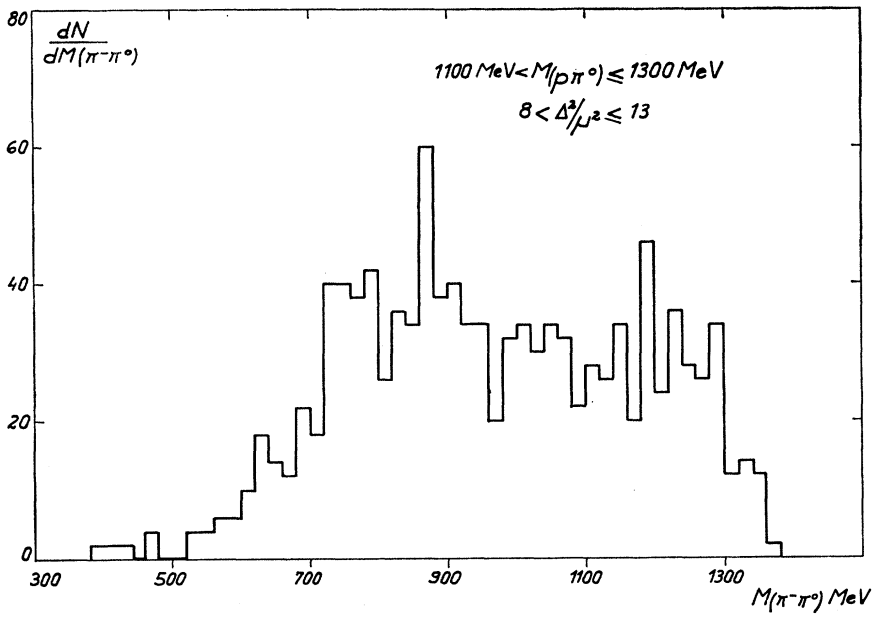


FIG. 8. ($\pi^-\pi^0$) mass spectrum for $8<\Delta^2/\mu^2\leqslant 13$ and in the $N^{*+}(1236)$ isobar region ($1100<M_{p\pi^0}\leqslant 1300$ MeV).

755±5 MeV with a width of 110±9 MeV.[4] This difference in the mass value shows clearly that one should not strictly deduce the $\rho^-$ mass and width from the mass spectra, but that these are only an indication of the parameters of the resonance. Moreover, it should be noticed that the mass and the width of the $\rho^-$ meson depend on the Breit-Wigner formula chosen.[14]

### B. Isobar Production

As one can see on Fig. 4, reaction (1) is strongly dominated by the $\rho^-$ production for $\Delta^2\leqslant 13\mu^2$. This may be observed on the different Dalitz diagrams [Figs. 5(a)–5(d)], where $M(p\pi^-)^2/\mu^2$ is plotted versus the $M(p\pi^0)^2/\mu^2$. In addition, on Fig. 5(c), an accumulation of events appears in the $N^{*+}(1236)$ isobar region.

The different $N\pi$ mass projections are shown on Figs. 6(a)–6(c) and 7(a)–7(c). The curves fitted on these distributions are obtained by taking into account the $\pi N$ phase space and the reflection of the $\rho^-$ production.[15] There is evidence for some $N^{*+}(1236)$ isobar production at the higher values of $\Delta^2$ [Fig. 6(c)]. Its production rate is estimated to be about 4% of the total of reaction (1) for $\Delta^2\leqslant 13\mu^2$, while that of the $\rho^-$ is of the order of 77%. The absence of $\rho^-$ in the $N^{*+}(1236)$ mass region (Fig. 8) indicates that there is no reflection of the $N^*(1236)$ on the $\rho^-$ and that the two channels

$$\pi^- p \to p\rho^- \quad \text{and} \quad \pi^- p \to \pi^- N^{*+}(1236)$$

are perfectly separated.

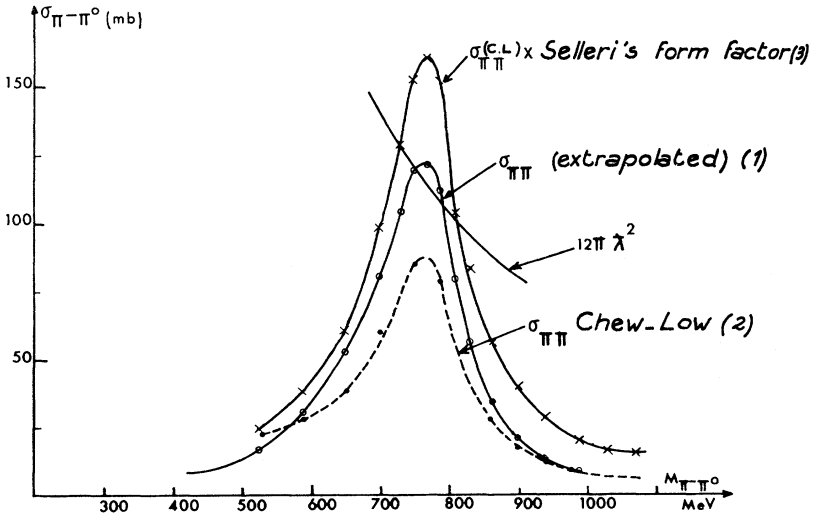


FIG. 9. ($\pi^-\pi^0$) elastic cross section as a function of the dipion mass. The unitary limit for a $l=1$ wave $[4\pi(2l+1)\lambda^2]$ is represented by a solid curve. ●, values obtained from the Chew-Low formula used in the physical region; ○, values obtained by extrapolation at $\Delta^2=-\mu^2$; ×, values obtained in the physical region by Chew-Low formula, modified by Selleri's form factor.

[14] J. P. Baton and G. Laurens, Phys. Letters **26B**, 471 (1968).

[15] The bad fit of these curves to the $p\pi^-$ mass spectrum comes from the additional reflection of the $N^{*+}(1238)$ isobar which is not taken into account here.

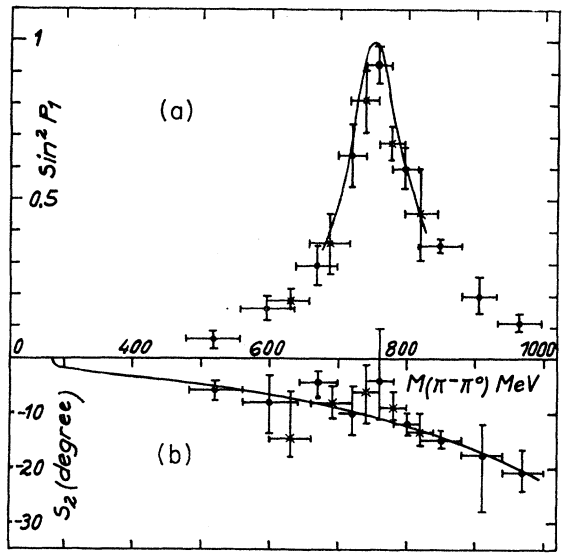


FIG. 10. (a) Values of $\sin^2 P_1$ as a function of the dipion mass. The solid curve represents a Breit-Wigner formula (8) fitted by least squares on the experimental points. The points and crosses represent two different choices of the mass intervals. (b) $S_2$ phase shift, in degrees, as a function of the dipion mass. The solid curve corresponds to the effective range formula (9). The points and crosses represent two different choices of mass intervals.

All these results are in agreement with those found previously at the same energy.[13] Nevertheless, we do not see the $N^{*0}(1688)$ isobar. Its absence may be explained by the very restricted range of $\Delta^2$ chosen for our study.

## V. PION-PION SCATTERING CROSS SECTION

A detailed study of the pion-pion elastic scattering was described in a previous paper.[4] Let us mention that the statistical accuracy has allowed to carry out in good conditions the extrapolation suggested by Chew and Low.[1] The pion-pion total elastic cross section at the pole of the transition matrix element has been obtained by extrapolating to $\Delta^2=-\mu^2$ the values of the function

$$F(W,\omega,\Delta^2)=\frac{2\pi}{f^2}\frac{k_{\rm lab}^2}{\omega(\frac{1}{4}\omega^2-\mu^2)^{1/2}}(\Delta^2+\mu^2)^2\frac{\partial^2\sigma}{\partial\omega^2\partial\Delta^2}, \quad (6)$$

where $W$ represents the total energy of the reaction (1) in the over-all c.m. system, $f^2$ is the pion-nucleon coupling constant, $k_{\rm lab}$ is the momentum of the incident pion in the laboratory system, and $\omega$ is the mass of the final dipion. We can represent this function by the following expression[16]:

$$F(W,\omega,\Delta^2)=\frac{-\Delta^2}{\mu^2}(\sigma_{\pi\pi}(\omega)+\sum_{n=1}^{\infty}C_n(\omega)(\Delta^2+\mu^2)^n)+\sum_{n=1}^{\infty}D_n(W,\omega)(\Delta^2+\mu^2)^n. \quad (7)$$

[16] J. Naisse and J. Reignier, Fortschr. Phys. 12, 523 (1964).

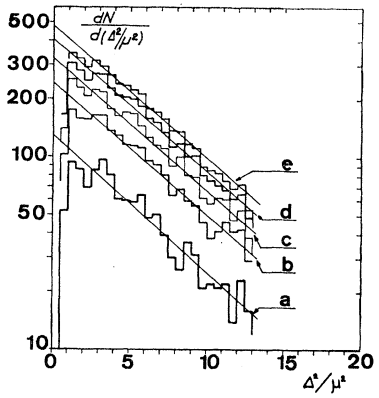


FIG. 11. $dN/d\Delta^2$ values for different $\rho^-$ mass intervals; straight lines have been fitted to the data by least squares. (a) $740<M_{\pi^-\pi^0}\leqslant 780$ MeV, (b) $720<M_{\pi^-\pi^0}\leqslant 800$ MeV, (c) $700<M_{\pi^-\pi^0}\leqslant 820$ MeV, (d) $680<M_{\pi^-\pi^0}\leqslant 840$ MeV, (e) $660<M_{\pi^-\pi^0}\leqslant 860$ MeV.

Figure 9, curve 1, shows the results of this extrapolation, limited to the first term of Eq. (7).[17] By this method the theoretical value of $12\pi\lambda^2$ expected by the unitarity limit for a resonant $P$ wave is reached.

On Fig. 9 are shown also the pion-pion elastic cross section obtained by the usual calculation in the physical region,[5,18,19] i.e., the mean value on a $\Delta^2$ interval (dashed curve), as well as the one obtained by the introduction of Selleri's form factor (curve 3). One notices the poor agreement of these two curves with the values obtained by extrapolation.

By a similar extrapolation of the dipion decay angular distributions, we have obtained the phase shift of the $P_1$ and $S_2$ waves (indices correspond to isobaric spin). These phase shifts are plotted as a function of the dipion mass on Fig. 10. The $P_1$ wave goes through 90° in the vicinity of 755 MeV, and the phase shift of the $S_2$ wave is small (less than 20°) and negative.

The local representation of $\sin^2 P_1$ by a Breit-Wigner formula,

$$\sin^2 P_1=\frac{(\Gamma/2)^2}{(\Gamma/2)^2+(\omega-\omega_r)^2}, \quad (8)$$

gives, for the $\rho^-$ width,

$$\Gamma=110\pm 9 \text{ MeV},$$

and for the $\rho^-$ mass,

$$\omega_r=755\pm 5 \text{ MeV}.$$

Figure 10(b) shows the graphic representation of $S_2$ by an effective-range formula

$$k\cot S_2=-1/a_2+\tfrac{1}{2}r_2k^2, \quad (9)$$

[17] A sufficient condition for neglecting the last terms of Eq. (17) at $\Delta^2=0$ is that the phenomenon is peripheral. This is, however, not necessary and we have called this hypothesis the "pseudo-peripheralism"; see Refs. 4 and 16 for details.

[18] Saclay-Orsay-Bari-Bologna Collaboration, Nuovo Cimento 29, 515 (1963).

[19] Saclay-Orsay-Bari-Bologna Collaboration, Nuovo Cimento 35, 713 (1965).

TABLE II. Slope of $dN/d(\Delta^2/\mu^2)$ for different $(\pi^-\pi^0)$ mass intervals.

| $\rho^-$ mass (MeV) | 740–780 | 720–800 | 700–820 | 680–840 | 660–860 | $\leqslant 660$ | $\geqslant 860$ |
|---|---|---|---|---|---|---|---|
| Slope of $dN/d\Delta^2$ | 8.6±0.4 | 8.0±0.3 | 8.2±0.2 | 8.2±0.2 | 7.8±0.1 | 3.9±0.2 | 5.1±0.1 |

where $k=(\frac{1}{4}\omega^2-\mu^2)^{1/2}$ is the relative momentum of the two pions in the dipion barycentric system; we obtain for the scattering length

$$a_2=0.073\pm0.007 \text{ fm},$$

and for the effective range

$$r_2=2.7\pm0.5 \text{ fm}.$$

## VI. PRODUCTION AND DECAY OF $\varrho^-$

Owing to the lack of statistics, the study of the production and decay of the $\rho^-$ meson has been done until now by taking a wide mass interval—generally 200 MeV. It was thus impossible to analyze whether the different parameters, production angle, matrix density elements, etc., were dependent on the choice of the dipion mass interval. A much higher statistics has allowed us to examine this point.

### A. $\varrho^-$ Production Angle

It is known that the $\rho^-$ production angular distribution follows an exponential law of the form $d\sigma/d\Delta^2 = Ae^{-B\Delta^2}$. Figure 11 shows a semilog plot of $dN/d(\Delta^2/\mu^2)$ versus $\Delta^2/\mu^2$ for intervals of increasing width around the $\rho^-$ central value. The slope of the curves fitted by least squares on the different distributions gives the

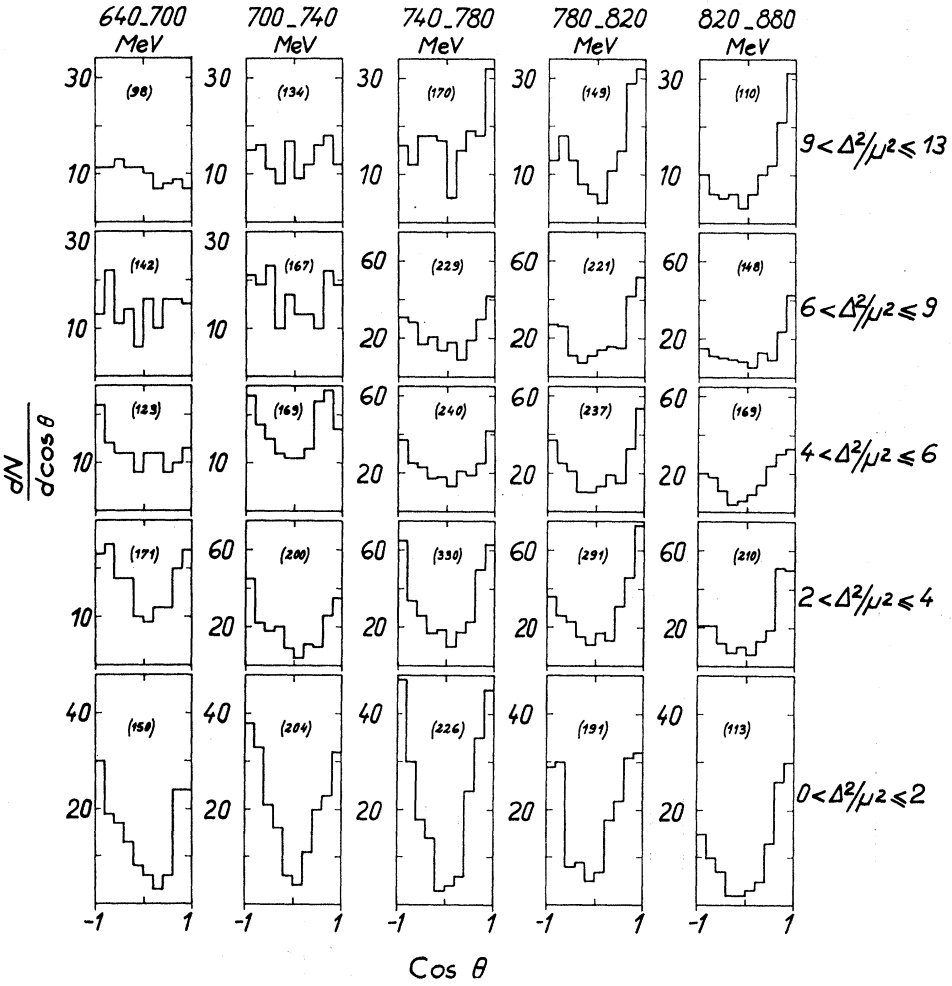


FIG. 12. Distributions of the $(\pi^-\pi^0)$ scattering angle in the $(\pi^-\pi^0)$ rest frame, for different dipion mass intervals and for different $\Delta^2$ cuts. In parentheses, the number of events in each distribution.

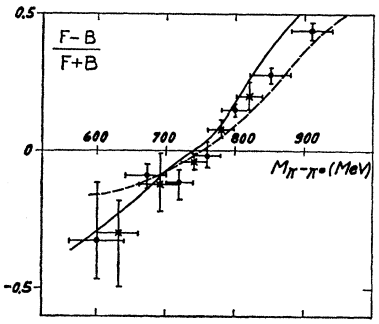


FIG. 13. Asymmetry parameter, as a function of the $(\pi^-\pi^0)$ mass. Experimental points are obtained by extrapolation; the solid curve represents the mean value of the asymmetry for $1 \leqslant \Delta^2/\mu^2 \leqslant 13$; the dashed curve represents the results obtained by a phase-shift analysis in the physical region (Ref. 22).

coefficient $B$. No significant variation of this slope is seen as function of the $\rho^-$ width. These results are tabulated in Table II. The mean value of the slope is $B=8.2\pm0.2$ $(\mathrm{GeV}/c)^{-2}$, which is in good agreement with the values quoted in other papers.[13,20] One notices that the slope of the nonresonant background is not constant. The following values have been found:

$$B'=3.9\pm0.2\ (\mathrm{GeV}/c)^{-2} \quad \text{for} \quad M_{\pi^-\pi^0} \leqslant 660\ \mathrm{MeV}$$

and

$$B'=5.1\pm0.1\ (\mathrm{GeV}/c)^{-2} \quad \text{for} \quad M_{\pi^-\pi^0} \geqslant 860\ \mathrm{MeV}.$$

This result gives some support to a quasi-two-body model of reaction (1) in the resonance region.[21]

On Fig. 11, where $\Delta^2$ distributions for different $\rho^-$ intervals are plotted, a depopulation is apparent for small values of $\Delta^2$; this is due to a scanning bias which consists in a lower detection efficiency for short proton tracks (less than 1 cm).

TABLE III. Probability for an isotropic Treiman-Yang angular distribution for different $\Delta^2/\mu^2$ and $(\pi^-\pi^0)$ mass intervals.

| $\Delta^2/\mu^2$ \ $\rho^-$ width (MeV) | 750–770 | 740–780 | 720–800 | 700–820 | 680–840 | 660–860 |
|---|---|---|---|---|---|---|
| 0– 2 | 0.60 | 0.80 | 0.25 | 0.25 | 0.10 | 0.10 |
| 2– 4 | 0.55 | 0.35 | 0.25 | 0.70 | 0.35 | 0.40 |
| 4– 6 | 0.45 | 0.30 | 0.03 | 0.08 | 0.07 | 0.20 |
| 6– 9 | 0.37 | 0.25 | 0.07 | 0.02 | 0.02 | 0.01 |
| 9–13 | 0.60 | 0.30 | 0.09 | 0.04 | 0.03 | 0.02 |

### B. $\pi^-\pi^0$ Scattering

Let us define the scattering angle $\theta_{\pi\pi}$ as the angle between the outgoing $\pi^-$ and the incoming $\pi^-$ in the barycentric system of final pions. Figure 12 shows the distributions of $\cos\theta_{\pi\pi}$ in the $\rho^-$ region for different $\Delta^2$ intervals. For the lowest values of $\Delta^2$, these angular distributions exhibit a familiar behavior: an excess of events in the backward direction for dipion masses less than 750 MeV, a symmetric distribution around 750 MeV, and a forward-peaked distribution for high dipion masses. However, when $\Delta^2$ increases, the shape of these distributions changes rapidly and becomes nearly isotropic for $9\mu^2<\Delta^2<13\mu^2$, except for an excess of events in the forward direction at the high mass values.

The asymmetry ratio $(F-B)/(F+B)=$(forward $-$backward)/(forward$+$backward) has been obtained at $\Delta^2=-\mu^2$, by extrapolating the coefficients of Legendre polynomials fitted on the angular distributions.[4] The values shown on Fig. 13 result from this extrapolation. The solid curve represents the mean values of this asymmetry ratio for $1\mu^2<\Delta^2<13\mu^2$, and the dashed curve has been obtained by phase-shift analysis from

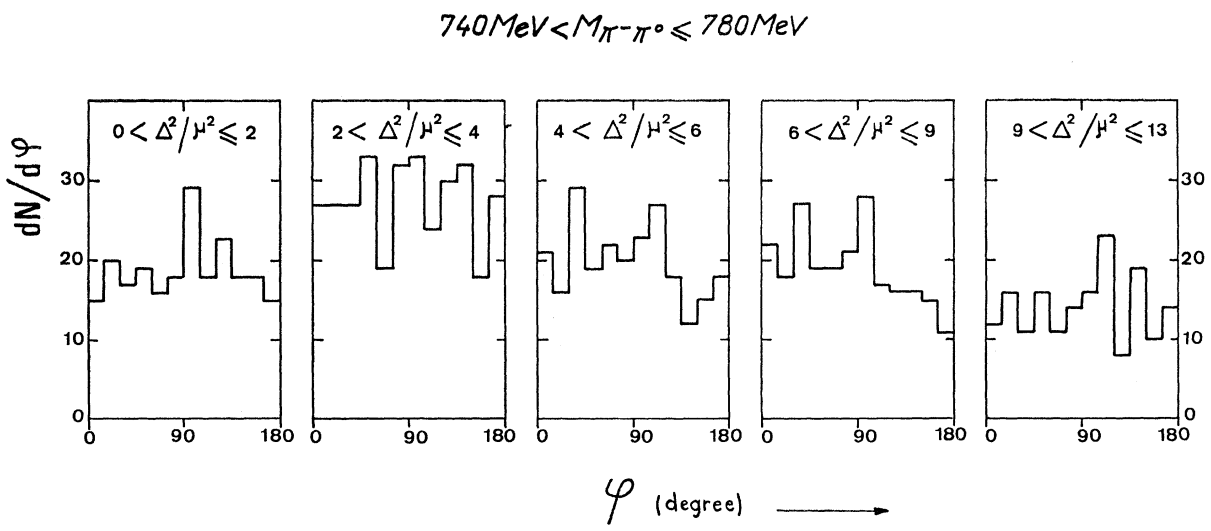


FIG. 14. Distribution of the Treiman-Yang angle for $740 < M_{\pi^-\pi^0} \leqslant 780$ MeV and for different $\Delta^2$ intervals.

[20] Birmingham-Bonn-Hamburg-London (I.C.)-München Collaboration, Nuovo Cimento 31, 729 (1964).
[21] D. R. O. Morrison, Phys. Letters 22, 226 (1966).

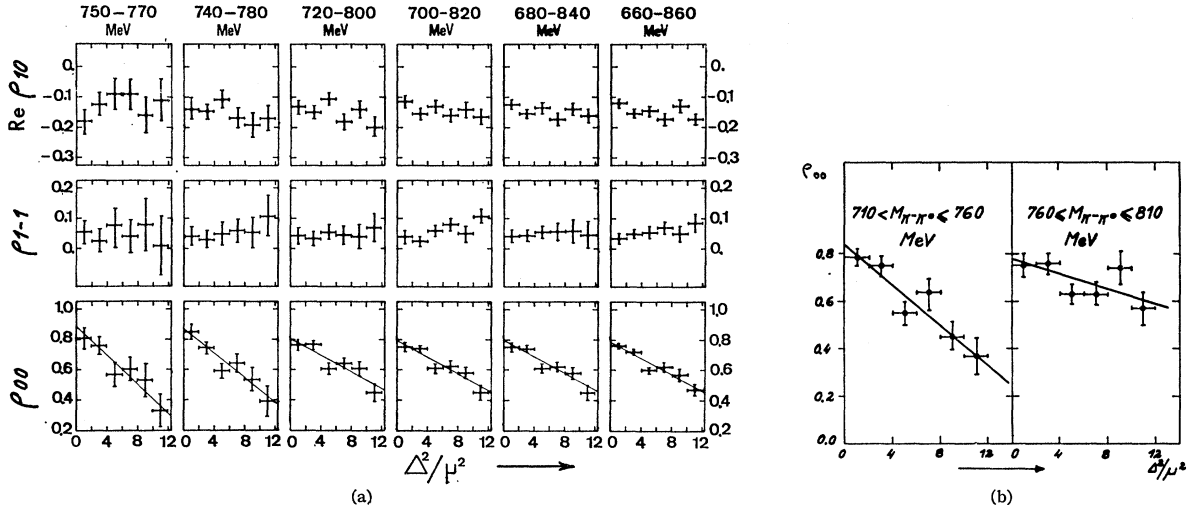


FIG. 15. (a) Values of the density matrix elements for the $\rho^-$ decay as a function of $\Delta^2$ for different $\rho^-$ mass intervals. (b) Values of $\rho_{00}$ density matrix element in the $\rho^-$ region.

a compilation.[22] There is good agreement between these curves and the values calculated at the pole. The asymmetry ratio is, therefore, one of the rare parameters of the pion-pion scattering which is insensitive to the extrapolation toward the pole.

### C. Treiman-Yang Test

If the single-pion production at low $\Delta^2$ is predominantly a one-pion-exchange mechanism, it is well known that the distribution in the dipion rest system of the angle between the plane defined by the incident and secondary $\pi^-$'s and the plane defined by the proton before and after interaction, must be isotropic. This angle can be defined by

$$\cos\varphi = \frac{\mathbf{p}_i \times \mathbf{q}_{\pi^-}}{|\mathbf{q}_i \times \mathbf{q}_{\pi^-}|} \frac{\mathbf{p}_1 \times \mathbf{p}_2}{|\mathbf{p}_1 \times \mathbf{p}_2|},$$

where $\mathbf{q}_i$, $\mathbf{q}_{\pi^-}$, $\mathbf{p}_1$, $\mathbf{p}_2$ are, respectively, the incident $\pi^-$ momentum, the secondary $\pi^-$ momentum, the proton momentum before interaction, and the proton momentum after interaction; all quantities are defined in the dipion rest system.

In Table III are tabulated the $\chi^2$ probability values given by a least-squares fit of an isotropic straight line to the Treiman-Yang angular distribution for different $\Delta^2$ and $\rho^-$ mass intervals. The agreement with an isotropic distribution is quite good for narrow $\rho^-$ intervals and for low $\Delta^2$. On the other hand, the agreement is very poor when the dipion interval and the $\Delta^2$ cut increase.

Figure 14 represents a set of these angular distributions for a dipon mass between 740 and 780 MeV.

### D. Angular Correlations

Study of angular correlations between the Treiman-Yang angle $\varphi$ and the scattering angle $\theta_{\pi\pi}$ provides additional information on the $\rho^-$ decay process.[23] With the assumption of a single resonant $P$ wave, they are related by the following expression, in terms of the density matrix elements:

$$W(\theta,\varphi) = (3/4\pi)[\rho_{00}\cos^2\theta + \tfrac{1}{2}(1-\rho_{00})\sin^2\theta - \mathrm{Re}\rho_{10}\sqrt{2}\sin 2\theta\cos\varphi - \rho_{1-1}\sin^2\theta\cos 2\varphi]. \quad (10)$$

It is known that, for a pure $\pi$ exchange mechanism and if the particle produced (the $\rho^-$) has $l=1$, one must have

$$\rho_{00}=1 \quad \text{and} \quad \rho_{10}=\rho_{1-1}=0.$$

On Fig. 15 are presented the values of the density matrix elements obtained by the method of moments for different $\rho^-$ mass intervals. The terms $\rho_{1-1}$ and $\mathrm{Re}\rho_{10}$ are small but different from zero for all the $\rho^-$ mass intervals considered.

TABLE IV. Slope and value at $\Delta^2=-\mu^2$ of the straight-line-fitted distribution of $\rho_{00}$ as a function of $\Delta^2$, for different $\rho^-$ mass intervals.

| $\rho^-$ width (MeV) | 750–770 | 740–780 | 720–800 | 700–820 | 680–840 | 660–860 | 710–760 | 760–820 |
|---|---|---|---|---|---|---|---|---|
| Slope of $\rho_{00}$ | 0.043±0.007 | 0.041±0.007 | 0.029±0.007 | 0.027±0.004 | 0.027±0.005 | 0.024±0.005 | 0.042±0.008 | 0.016±0.008 |
| $\rho_{00}$ value at $\Delta^2=-\mu^2$ | 0.94 ±0.04 | 0.91 ±0.04 | 0.84 ±0.04 | 0.82 ±0.02 | 0.82 ±0.03 | 0.79 ±0.03 | 0.88 ±0.04 | 0.79 ±0.04 |

[22] J. P. Baton and J. Reignier, Nuovo Cimento **36**, 1149 (1965).
[23] K. Gottfried and J. D. Jackson, Nuovo Cimento **33**, 309 (1964).

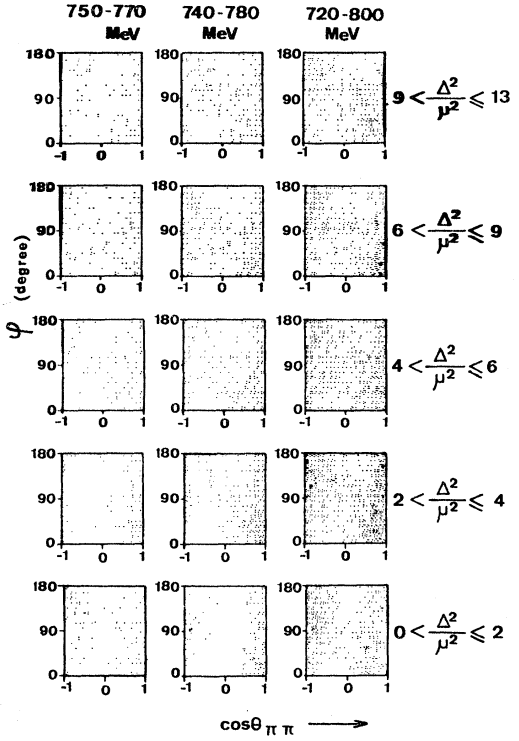


FIG. 16. Plots of the Treiman-Yang angle $\varphi$ versus the scattering angle $\cos\theta_{\pi\pi}$ for different $\rho^-$ mass intervals and $\Delta^2$ cuts.

A first-degree polynomial has been adjusted by least squares on the $\rho_{00}$ calculated values. It seems that the slope of this straight line and its value at $\Delta^2=-\mu^2$ decrease systematically when the $\rho^-$ mass interval increases (Table IV). In addition, the extrapolated value of this straight line at $\Delta^2=-\mu^2$ and its slope are different for the lower half of the $\rho^-$ meson ($710<M_\rho\leqslant 760$ MeV) or the upper half ($760<M_\rho\leqslant 810$ MeV) [Fig. 15(b)].

Finally (Fig. 16), a strong correlation between $\theta_{\pi\pi}$ and $\varphi$ is observed. This diagonal effect[12,19] persists for all $\rho^-$ mass interval and seems independent of the $\Delta^2$ cut. This corresponds to the presence of the $\mathrm{Re}\rho_{10}$ term. Table V summarizes the results, giving, for various $\rho^-$ mass intervals and $\Delta^2$ values, the ratio of the population in each quarter of the $\theta_{\pi\pi}$-$\varphi$ plot to the total population of the plot.

The different behavior of $\rho_{00}$ on the tails of the $\rho^-$ finds a reasonable explanation in the presence of a $T=2$, $D$ wave in the high mass region.

The sensitivity of the $\rho_{ij}$ matrix elements to the choice of the $\rho^-$ mass interval makes doubtful any physical interpretation of the experimental values of $\rho_{ij}$'s for wide resonances. This is *a fortiori* true when, in experiments with low statistics, one considers wide $\Delta^2$ or effective-mass intervals.

TABLE V. Ratios of the population in each quarter of the ($\varphi$, $\cos\theta_{\pi\pi}$) plot to the total population of the plot for different $\Delta^2$ and ($\pi^-\pi^0$) mass intervals. Values for the four quarters are displayed in each table entry as follows:

| | $-1\leqslant\cos\theta_{\pi\pi}<0$ | $0<\cos\theta_{\pi\pi}\leqslant 1$ |
|---|---|---|
| $90°<\varphi\leqslant 180°$ | ... | ... |
| $0°\leqslant\varphi< 90°$ | ... | ... |

The sum of the four entries is $N$.

| $\Delta^2/\mu^2$ \ $\rho^-$ width (MeV) | 750–770 | | 660–860 | |
|---|---|---|---|---|
| 0–2 | 0.36±0.08 | 0.17±0.06 | 0.30±0.02 | 0.20±0.03 |
| | 0.16±0.06 | 0.31±0.08 | 0.19±0.03 | 0.32±0.02 |
| 2–4 | 0.27±0.07 | 0.19±0.05 | 0.30±0.02 | 0.21±0.03 |
| | 0.23±0.05 | 0.30±0.08 | 0.16±0.03 | 0.33±0.02 |
| 4–6 | 0.28±0.05 | 0.20±0.04 | 0.28±0.02 | 0.21±0.02 |
| | 0.20±0.04 | 0.31±0.06 | 0.17±0.03 | 0.33±0.02 |
| 6–9 | 0.25±0.05 | 0.20±0.04 | 0.29±0.02 | 0.19±0.03 |
| | 0.19±0.04 | 0.35±0.05 | 0.15±0.02 | 0.36±0.02 |
| 9–13 | 0.29±0.06 | 0.24±0.04 | 0.28±0.03 | 0.20±0.03 |
| | 0.22±0.03 | 0.25±0.06 | 0.16±0.03 | 0.36±0.02 |

## VII. CONCLUSIONS

The results obtained show that the OPE model can be considered as a dominant mechanism for the reaction $\pi^-p\to\pi^-\pi^0p$ at the present energy. Owing to the fairly large statistics accumulated, we were in good position for analysis of the behavior of different $\rho^-$ parameters as a function of $\Delta^2$ and for different $\pi^-\pi^0$ intervals around the $\rho^-$ central value. It then appears that:

(a) The $\rho^-$ mass and width seem constant with respect to $\Delta^2$, when the kinematic corrections are taken into account.

(b) The slope of $\rho^-$ differential production cross section is constant, from narrow to wide $\pi^-\pi^0$ mass intervals. On the other hand, the slope of $\pi^-\pi^0$ differential cross section outside the $\rho^-$ region is different and smaller.

(c) The value of the $\rho_{00}$ density matrix element is strongly dependent of $\Delta^2$ and also, but less significantly, of the $\rho^-$ mass interval; in particular, the $\rho_{00}$ values are not the same in the two halves of the $\rho^-$ resonance.

(d) Angular correlations between Yang-Treiman angle and scattering angle persist for any $\Delta^2$ or mass cuts.

(e) Finally, the scattering angle $\theta_{\pi\pi}$ exhibits in the $\rho^-$ region the expected behavior of $\cos^2\theta_{\pi\pi}$ for very small values of $\Delta^2$; it becomes practically isotropic for $\Delta^2$ above $9\mu^2$.

## ACKNOWLEDGMENTS

We are particularly indebted to Professor A. Berthelot and Dr. A. Rogozinski for their interest and encouragement in this work. We are also very grateful to Professor J. Reignier and Dr. A. Morel for many useful discussions.